Diagnosing the systematic occurrence of wintertime compound climate extremes in North America and Europe

Gabriele Messori, Davide Faranda

Diagnosing the Systematic Occurrence of Wintertime Compound Climate Extremes in North America and Europe

Gabriele Messori[1,2] Davide Faranda[3,4,5]

1. Department of Earth Sciences and Centre of Natural Hazards and Disaster Science (CNDS), Uppsala University, Uppsala, Sweden.
2. Department of Meteorology and Bolin Centre for Climate Research, Stockholm University, Stockholm, Sweden.
3. Laboratoire des Sciences du Climat et de l'Environnement, LSCE/IPSL, CEA-CNRS-UVSQ, Université Paris-Saclay, Gif-sur-Yvette, France.
4. London Mathematical Laboratory, London, UK.
5. LMD/IPSL, Ecole Normale Superieure, PSL research University, Paris, France.

Corresponding author: Gabriele Messori (gabriele.messori@geo.uu.se)

Key Points:

- North American cold spells and European wet or windy extremes are very strongly coupled to recurrent large-scale atmospheric patterns.
- Compound cold–wet–windy anomalies in North America and Europe are closely connected and share common atmospheric circulation patterns.
- Compound cold–wet–windy extremes show a weaker connection than the anomalies, but are nonetheless linked.

Abstract

The repeated co-occurrence of cold spells over Eastern North America and wet or windy extremes over Western Continental Europe during recent winters, has led to hypothesise a link between the two. Here, we provide a systematic analysis of the interplay between the large-scale atmospheric circulation and co-occurring cold spells in North America and wet or windy extremes in Europe, which we collectively term compound cold–wet–windy extremes. We leverage a recent approach grounded in dynamical systems theory, which provides an analytically and computationally efficient analysis of spatially resolved, multivariate climate extremes. We find that there are specific, recurrent large-scale atmospheric circulation patterns systematically associated with co-occurring cold–wet–windy anomalies. Evidence for this is also found when focussing on compound cold–wet–windy extremes, although with a weaker signal. This motivates further analyses focussing specifically on the statistics and drivers of the compound extreme occurrences.

Plain Language Summary

In recent winters, very cold weather over the eastern part of North America and stormy weather or heavy rainfall in Europe have often made the news. One may think that these events are independent, since they occur several thousands of kilometres apart. However, researchers have hypothesised that there may be weather patterns that connect these different weather episodes. Here we test this idea. We find that there is indeed a connection between unusually cold weather in Eastern North America and unusually stormy weather and heavy rainfall in Western Continental Europe. We also find a link, albeit weaker, when focussing specifically on extreme events – namely only the coldest of the cold spells, the windiest of the storm days and the wettest of the heavy rainfall days. The strongest connection, however, emerges when looking at unusual but not extreme weather episodes.

1 Introduction

During recent winters, ostensibly frequent cold spells in Eastern North America and wet or windy extremes in Western Continental Europe have garnered widespread scientific attention (e.g. Palmer 2014; Lee et al., 2015; Matthias and Kretschmer, 2020; van Oldenborgh et al., 2015; Hillier and Dixon, 2020; Owen et al., 2021). The two event classes have typically been discussed separately. However, their repeated co-occurrence has led to hypothesise that these are spatially compounding extremes, namely extremes that occur at geographically remote locations but are associated with common physical drivers. Specifically, Messori et al. (2016) argued for a link mediated by large-scale atmospheric circulation anomalies over the North Atlantic. They conditioned their analysis on Eastern North American cold spells, finding that these matched positive precipitation and wind anomalies over parts of Europe. However, extreme wet or windy weather in Europe was not investigated. A later study by De Luca et al. (2020) focussed on co-occurring cold extremes in North America and wet extremes in Europe, providing partial support for the hypothesis of Messori et al. (2016). The study used an approach similar to the one we will adopt here, yet did not consider variables associated with the large-scale atmospheric circulation nor wind extremes in Europe. The current understanding of co-occurring cold spells in North America and wet or windy extremes in Europe, which we collectively term compound cold–wet–windy extremes, is thus incomplete. Filling this knowledge gap is all the more urgent in view of the growing awareness of the relevance of compound extremes, whose impacts often exceed the sum of those due to the individual events comprising them (Zscheischler et al., 2018).

The multivariate perspective inherent to compound extremes, adds complexity to conventional statistical tools for the study of extremes (Naveau, 2005). A wide range of approaches have been proposed to deal with multivariate extreme value statistics in climate data, from copula-based methods to max-stable models, conditional exceedance models, machine learning algorithms and more (e.g. Oesting and Stein, 2018; Brunner et al., 2019; Tavakol et al., 2020; Towler et al., 2020; Vogel et al., 2021). Spatially compounding extremes, such as the ones we consider here, present the additional challenge of how to incorporate spatial information in the analysis. Some of the above multivariate statistical approaches may be extended to incorporate spatial information, but this often results in highly complex models (e.g. Genton, 2015; Liu et al., 2021).

Here, we leverage dynamical systems theory to provide an analytically and computationally efficient, spatially resolved analysis of compound cold–wet–windy extremes in North America and Europe. The approach builds upon recent advances in dynamical systems theory (Faranda et al., 2020a), and allows to compute a metric reflecting the instantaneous coupling between different atmospheric variables, which we term co-recurrence ratio, or α. In this study, we extend this approach for the first time beyond the bivariate case. We propose this as an effective complement to existing analyses of spatially compounding extremes, which may support our understanding of the interplay between different climate extremes and their physical drivers.

Motivated by the incomplete knowledge on compound cold–wet–windy extremes in North America and Europe, we specifically seek to answer the following questions:

(i) Do cold spells over Eastern North America and wet or windy extremes over Western Continental Europe individually emerge as events with a particularly strong coupling to large-scale circulation patterns?

(ii) Is there evidence for recurrent large-scale circulation patterns systematically associated with the co-occurrence of these extremes?

Concerning the first question, there is a vast literature dealing with large-scale circulation patterns favouring the extremes analysed here (e.g. Haylock and Goodess, 2004; Cellitti et al., 2006; Donat et al., 2010; Grotjahn et al., 2015; Harnik et al., 2016; Smith and Sheridan, 2018; Laurila et al., 2021). However, the question of whether the coupling of these extremes with the large-scale circulation is unusually strong relative to other days has not been addressed (with the exception of an exploratory analysis for North America in Faranda et al., 2020a). Concerning the second question, Messori et al. (2016) conditioned their large-scale atmospheric analysis only on cold spells in Eastern North America, without accounting for European extremes. We begin by analysing separately North America and Europe, and then consider a multivariate analysis explicitly addressing the spatially compounding nature of the cold–wet–windy extremes.

2 Data

We use ECMWF's ERA5 reanalysis data, over boreal winter (December–January–February, DJF) 1979–2020 and with a horizontal resolution of 0.5° (Hersbach *et al.*, 2020). We compute

daily averages from hourly data for surface variables and 6-hourly data for pressure-level variables. Anomalies are defined relative to a smoothed daily climatology (using a 15-day running mean, similar to Harnik *et al.*, 2016). Extreme events are diagnosed using anomalies of 2-metre temperature (t2m), 10-metre wind (10m wind) and total precipitation (tp). Large-scale atmospheric patterns are diagnosed using sea-level pressure (SLP). We chose this over geopotential height, as the latter displays long-term trends that could affect our dynamical systems analysis (Faranda *et al.*, 2020b).

The t2m in North America is analysed over 30–45 °N 260–290 °E (grey box in Fig. 1a), while 10-m wind and precipitation in Europe are analysed over 45–60 °N 350–20 °E (grey box in Fig. 2a). These domains approximately follow those used in Messori *et al.* (2016) for Eastern North American cold spells and the area of high windstorm occurrence in Western Continental Europe identified in Hanley and Caballero (2012), respectively. The same domains are also used for analysing SLP co-recurrences (see Sect. 3). A sensitivity analysis using larger domains is presented in the Supplementary Material. To avoid double-counting cold spells, we impose a minimum separation of 5 days between successive events, following Messori *et al.* (2022). A similar minimum separation is imposed when selecting high α days and when selecting single-gridbox extremes. Unless otherwise specified, all figures are computed for the 50 most extreme events.

Unless otherwise specified, we test statistical significance of composites by verifying whether at least 2/3 of composite members have the same sign. This provides an indication of the coherence of the signal across composite members. Assuming a binomial formula with equal chances for positive and negative anomalies, the probability of obtaining a greater than 2/3 sign agreement randomly is well below 5%.

3 Diagnosing the Coupling of Atmospheric Variables

Our analysis rests on an indicator of the instantaneous coupling of multiple atmospheric variables, termed *co-recurrence ratio*, or α (Faranda *et al.*, 2020a; see also applications in De Luca *et al.*, 2020a,b and Messori and Faranda, 2021). Given two variables drawn from a chaotic dynamical system, α measures the extent to which recurrences in one variable correspond to recurrences in the other. For example, α computed for SLP and t2m over a given geographical

domain, diagnoses how often, given the recurrence of a specific t2m spatial pattern in the domain, one also observes the recurrence of the associated SLP spatial pattern. In other words, if α at a given timestep t in our dataset is large, then every time a t2m pattern similar to the t2m pattern of time t appears in the dataset (a *recurrence*), then the SLP pattern at that other time will also resemble the SLP pattern of time t. This may then be interpreted as a high coupling. The converse holds for low α. The co-recurrence ratio may also be computed for more than two variables. In this case, it diagnoses the extent to which one observes simultaneous recurrences of all the variables being considered. When computing α for more than two variables, one is thus imposing additional constraints relative to the bivariate case. We therefore expect a trivariate α to display lower values than its bivariate counterpart.

Unlike other statistical coupling measures, α is instantaneous in time (local in phase space). This implies that a value of α is obtained for each timestep in the dataset being analysed. Since α is independent of the ordering of the variables, it may not be interpreted in terms of causality. The range of the co-recurrence ratio is $0 \leq \alpha \leq 1$. We provide the details of the calculation of α for climate data in Text S1.

4 Large-scale drivers of cold spells in Eastern North America and wet or windy extremes in Western Continental Europe

4.1 An Analysis of Individual Extreme Event Classes

We first study separately cold spells in Eastern North America and wet or windy extremes in Western Continental Europe. To verify how these extremes couple to large-scale atmospheric patterns, we compute α between the relevant impact variable and SLP (see Sect. 2). We begin by analysing days on which t2m in North America is highly coupled to SLP. The 50 days with the highest coupling display an anomalous high pressure centred to the south-west of the Great Lakes region, flanked by two negative pressure anomaly cores (Fig. 1a; *cf.* Faranda *et al.*, 2020a). This tripole favours oceanic airmass advection and warm anomalies over Alaska, and at the same time northerly advection of cold high-latitude air further to the east. Anomalies in excess of -10 K are attained over the eastern part of the continent, even though we are conditioning solely on α. The large-scale pattern is remarkably similar to that obtained by conditioning on the 50 coldest spells in Eastern North America (Fig. S1a), and resembles the spatial patterns found by previous studies investigating North American cold spells (*e.g.* Cellitti

et al., 2006; Messori *et al.*, 2016; Harnik *et al.*, 2016; Smith and Sheridan, 2018). Additionally, the 50 days with the highest coupling between SLP and t2m show an anomalously frequent occurrence of cold spells over a broad swath of North America (Fig. S2a). Finally, we compute the $\alpha_{t2m,SLP}$ anomalies associated with the 50 coldest spells defined at each individual gridbox (Fig. 1b). The region that shows negative temperature anomalies in Figs. 1a, S1a also displays positive $\alpha_{t2m,SLP}$ anomalies in Fig. 1b. Thus, α shows that the cold spells share a similar spatial footprint and are systematically associated with a recurrent SLP configuration. We conclude that the occurrence of cold spells in Eastern North America is systematically associated with a stronger than usual coupling between SLP and t2m. The qualitative results are not dependent on the choice of computing $\alpha_{t2m,SLP}$ by using the same geographical domain for both variables. Indeed, if we compute $\alpha_{t2m,SLP}$ using t2m over the cold spell box and the SLP pattern over a much larger North American domain, the results are qualitatively comparable (Fig. S3).

We next shift the focus to 10m wind and tp anomalies in Europe. The 50 days with the highest coupling between 10m wind and SLP display strong positive 10m wind anomalies over Western Continental Europe and an SLP anomaly dipole with a strong negative core to the south-east of Iceland and a weaker positive core over the western Mediterranean (Fig. 2a). This eastward-shifted, NAO-like dipole is typically associated with a zonalised and intensified jet stream, which in turn results in heightened cyclone frequency and wind destructiveness over Western Europe (Donat *et al.*, 2010; Hanley and Caballero, 2012; Gómara *et al.*, 2014; Messori and Caballero 2015; Messori *et al.*, 2019). A similar SLP anomaly pattern, albeit with a northward-eastward shifted positive SLP core, is found for the 50 days with the highest coupling between tp and SLP (Fig. 2b). Because of the shift in the SLP core, the positive tp anomalies are also shifted slightly northwards relative to the 10m wind anomalies. We reconduct the geographical overlap between the 10m wind and tp anomalies to the dominant role of North Atlantic extratropical cyclones in bringing both strong winds and heavy precipitation to Western Europe, which in turn results in a close relationship between these two classes of extremes (De Luca *et al.*, 2020a; Owen *et al.*, 2021). This relationship emerges here in the form of a high coupling between SLP patterns favouring the presence of cyclones over the continent (see references above) and large 10m wind and tp anomalies there. These SLP, tp and 10m wind anomaly patterns are additionally very similar to those conditioned on the occurrence of tp or 10m wind extremes in the region of interest (Fig. S1b, c).

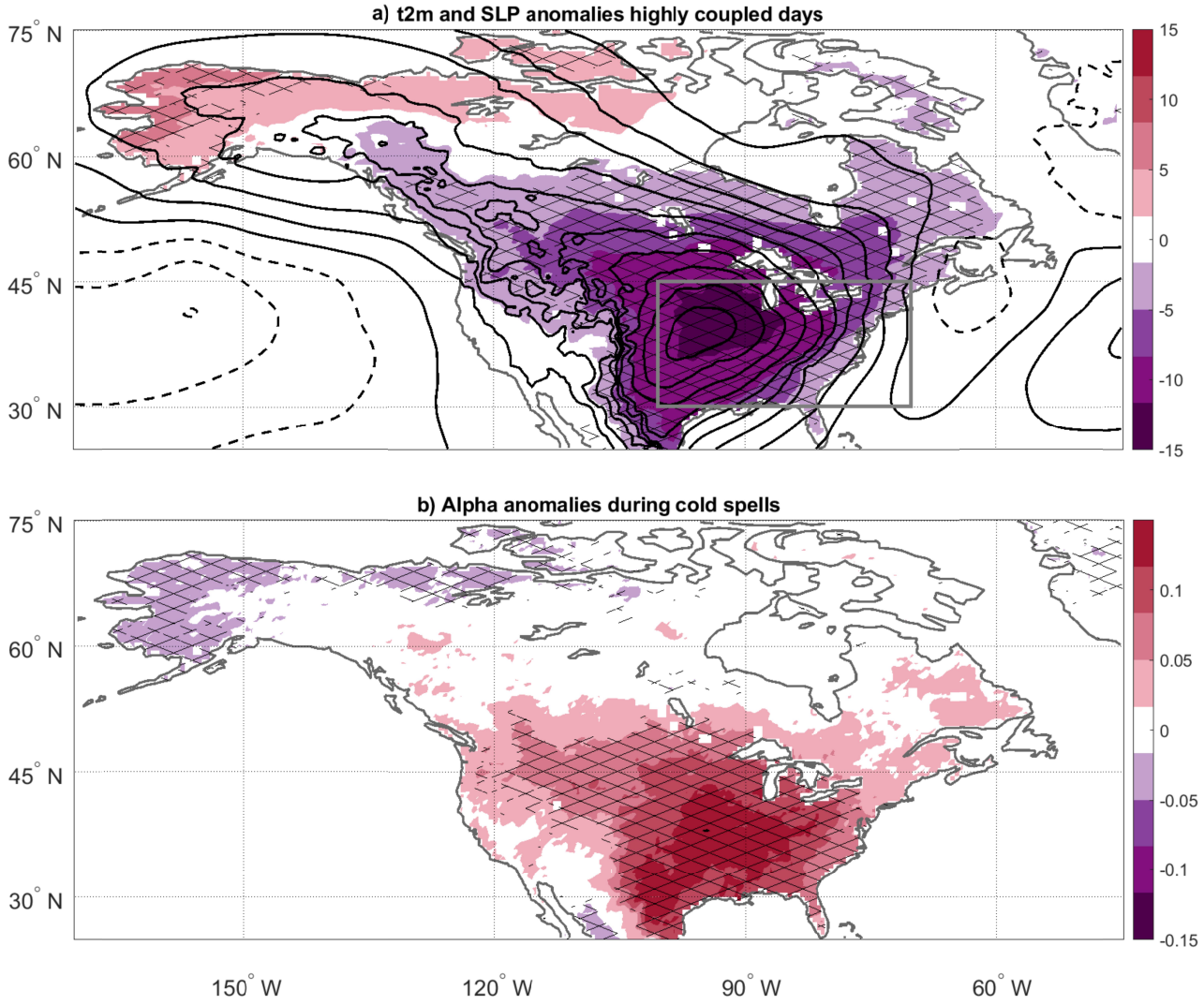

Figure 1. Cold spells and high t2m–SLP coupling days in North America. (a) t2m (K, colours) and SLP (hPa, contours) anomalies for the 50 days displaying the highest $\alpha_{t2m,SLP}$. (b) Anomalies in $\alpha_{t2m,SLP}$ observed during the 50 coldest spells at each gridbox. SLP contours in (a) are every 2 hPa (negative dashed). Cross-hatching marks regions where at least two thirds of the (a) t2m and (c) $\alpha_{t2m,SLP}$ anomalies share the same sign. All α are computed over 30–45 °N 260–290 °E (grey box in (a)).

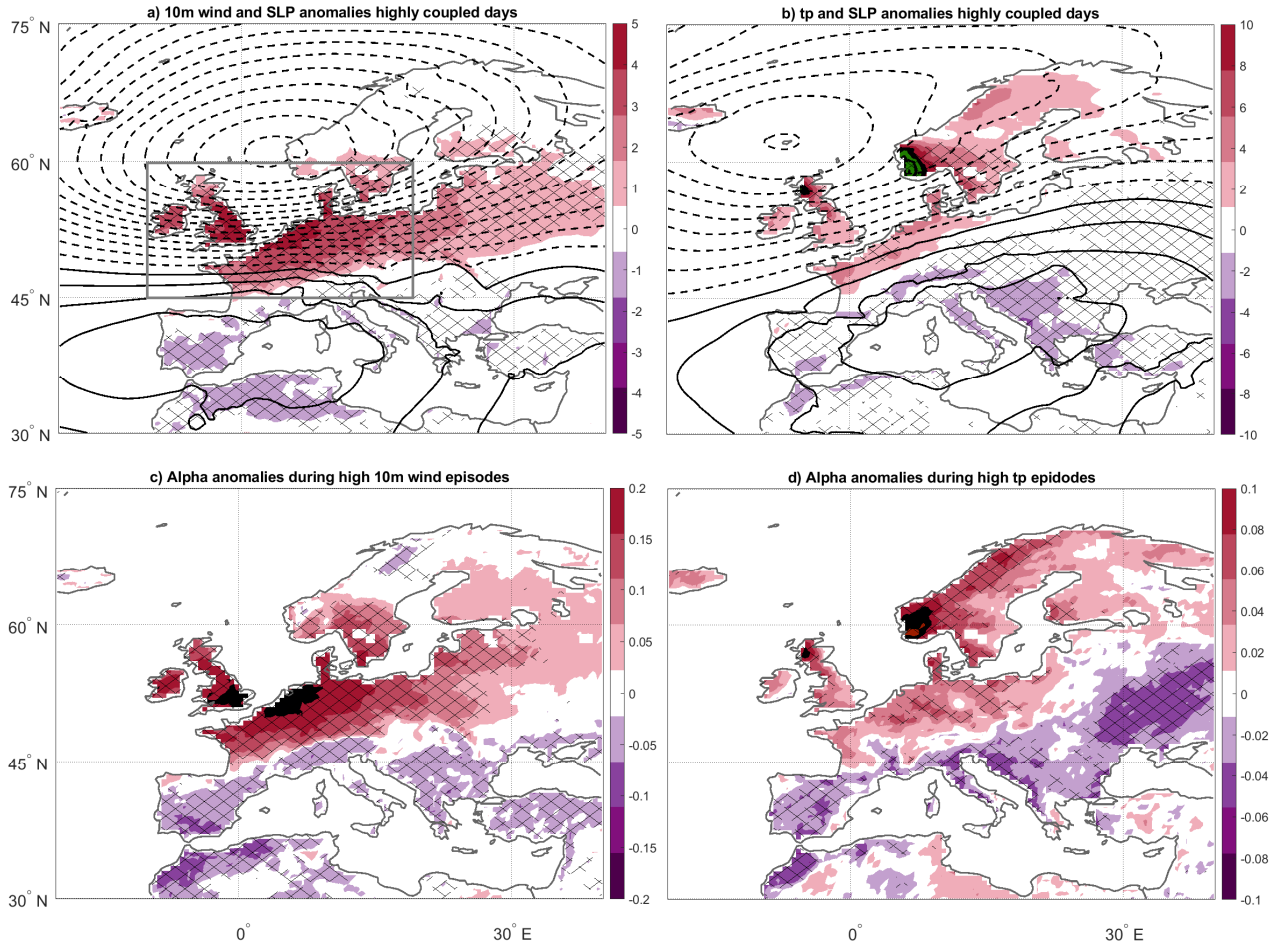

209

210 **Figure 2.** Extremes in 10m wind and tp and days with high 10m wind or tp coupling with SLP in
211 Europe. (a)10m wind (m s^{-1}, colours) and SLP (hPa, contours) anomalies during the 50 days
212 displaying the highest $\alpha_{10m\_wind,SLP}$ over Europe. (b) Same as (a) but for tp (mm day^{-1}) during the
213 50 days displaying the highest $\alpha_{tp,SLP}$. (c) Anomalies in $\alpha_{10m\_wind,SLP}$ observed during the 50
214 strongest 10m wind events at each gridbox. (d) Anomalies in $\alpha_{tp,SLP}$ observed during the 50
215 strongest tp events at each gridbox. SLP contours in (a, b) are every 2 hPa (negative dashed).
216 Cross-hatching marks regions where at least two thirds of the anomalies shown in colours share
217 the same sign. Days with no precipitation are not included in the latter calculation. The colour
218 ranges in c, d differ. All α are computed over 45–60 °N 350–20 °E (grey box in (a)).
219
220 We indeed find that the 50 highest coupling days between SLP and the two impact variables
221 correspond to an anomalously high occurrence of 10m wind and tp extremes over regions similar
222 to those highlighted in Fig. 2 (Fig. S2b, c). The regions that show strong positive 10m wind and
223 precipitation anomalies in Fig. 2a,b also display positive $\alpha_{10m\_wind,SLP}$ and $\alpha_{tp,SLP}$ anomalies during
224 extremes in the former variables (Fig. 2c, d). In analogy with the cold spells analysis, we
225 interpret this as meaning that the surface wind and precipitation extremes in Western Continental

Europe share common spatial footprints and are systematically associated with recurrent SLP configurations. These configurations are similar for the two classes of extremes. We conclude that the occurrence of wet or windy extremes in Western Continental Europe is associated with a stronger than usual coupling between SLP and the relevant impact variable. Again, using a larger SLP domain for computing $\alpha_{10m\_wind,SLP}$ and $\alpha_{tp,SLP}$ provides qualitatively comparable results (Fig. S4).

4.2 Compound Cold–Wet–Windy Extremes

We next consider the link between the cold spells over Eastern North America and the wet or windy extremes over Western Continental Europe. In Sect. 4.1, we showed that the individual extreme classes display a close coupling of the relevant impact variable with the atmospheric circulation as diagnosed by SLP. If the North American and European extremes are indeed linked through a common large-scale circulation anomaly pattern, we would expect that occurrences of compound cold–wet–windy extremes should match high coupling events between the SLP patterns in the two continents. We thus compute α between North American and European SLP fields. For the 50 highest coupling days, both the SLP anomalies and the t2m, 10m wind and tp anomalies qualitatively match those discussed in Sect. 4.1 (*cf.* Fig. 3a, b with Figs. 1a and 2a, b). The most notable difference is the absence in Fig. 3a, b of weak negative SLP anomalies flanking the North American cold spells. However, the key SLP structures such as the anomalous high over central-eastern North America and the dipole over Europe are very closely reproduced. Similarly, the t2m, 10m wind and tp anomalies only show minor qualitative differences (*e.g.* in central-northern Canada), although they are systematically weaker in magnitude. The same qualitative picture holds if continental-scale domains are used to compute α between North American and European SLPs. However, the additional information given by the simultaneous enlargement of both the North American and European domains leads to the inclusion of SLP structures with little effect on the surface events of interests, and further dilutes the magnitude of the signal (Fig. S5a, b).

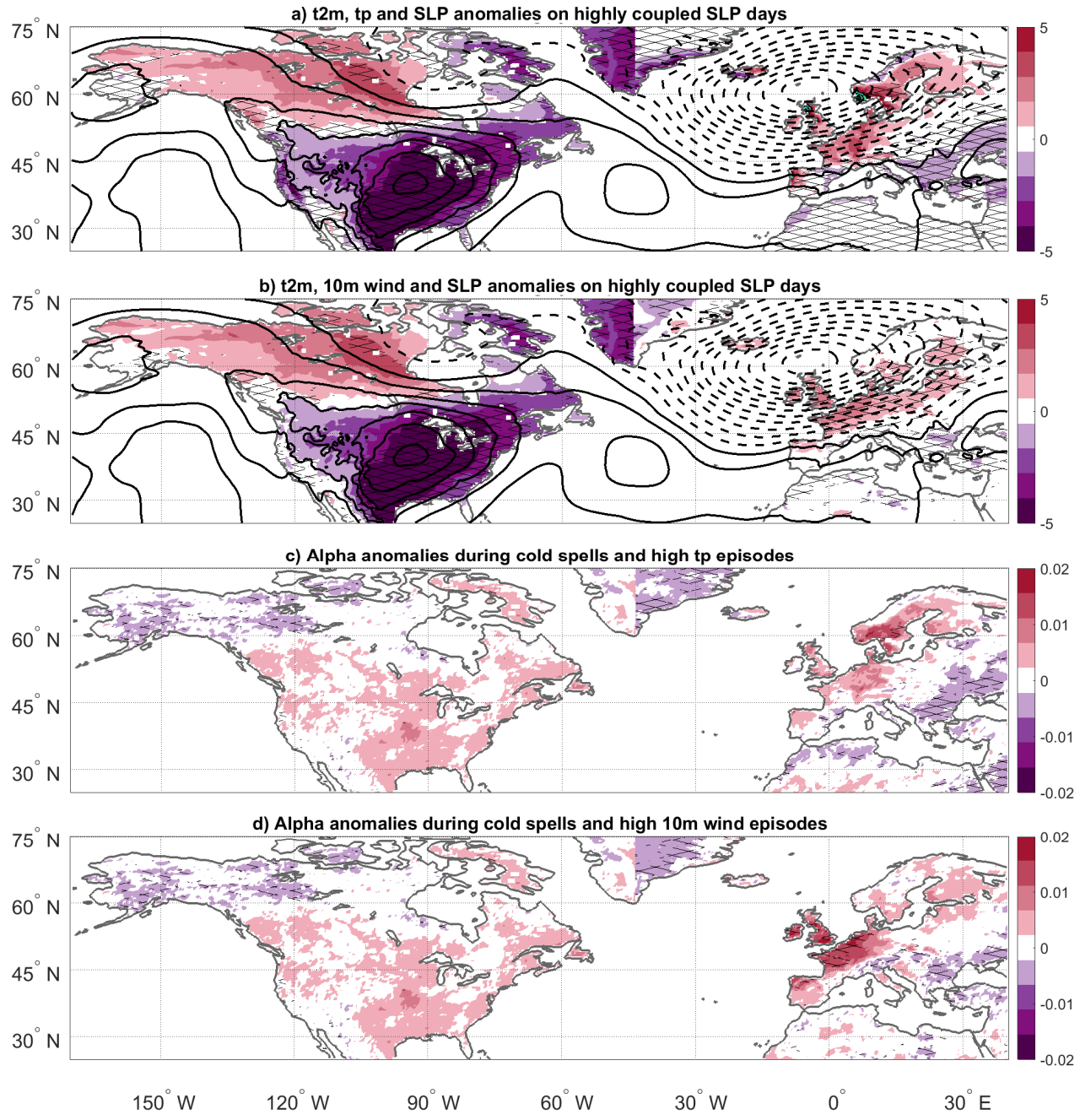

Figure 3. Surface extremes and days with high SLP coupling between North America and Europe. (a) t2m (K) and tp (mm day^{-1}) anomalies in colours in the left and right-hand sides of the panel, respectively. SLP (hPa) anomalies are shown in contours every 2 hPa (negative dashed). Anomalies are composited over the 50 days displaying the highest $\alpha_{SLP1,SLP2}$, where SLP1 is over 30–45 °N 260–290 °E and SLP2 is over 45–60 °N 350–20 °E. (b) Same as (a) but for 10-metre wind (10m wind, m s^{-1}, colours) in the right-hand side of the panel. (c) Anomalies in $\alpha_{SLP1,SLP2}$ observed during the 50 coldest spells or most extreme 10m wind events at each gridbox in the left and right-hand sides of the panel, respectively. (d) Same as (c) but for the 50 strongest tp events at each gridbox in the right-hand side of the panel. Cross-hatching marks regions where at least two thirds of the anomalies shown in colours share the same sign.

The high SLP coupling days between North America and Europe thus show a clear footprint in the surface anomalies. Moreover, the large-scale SLP patterns in Fig. 3a, b are comparable to those conditioned on the occurrence of compound cold–wet–windy extremes (Fig. S6). However, the link between the high SLP coupling days and the local extreme occurrences is considerably weaker than what observed for the monovariate extremes (*cf.* Figs. 1b, 2c, d and Fig. 3c, d). Specifically, the anomalies shown in Fig. 3c, d show limited sign agreement, pointing to a large case-by-case variability. The link between the high SLP coupling days and compound cold–wet–windy extremes is generally stronger in Europe than in North America, with the latter again showing limited sign agreement (Table S1).

There is thus mixed evidence for the existence of co-recurrent regional or continental-scale circulation patterns coupled to the compound cold-wet-windy extremes analysed here. This may be due to α in Fig. 3 being based only on SLP and not including any of the impact variables. We thus compute the trivariate co-recurrence for pairs of our impact variables (t2m and tp and t2m and 10m wind, respectively) and SLP in the respective domains. With the trivariate coupling, we are requiring a co-recurrence of SLP patterns and surface variable patterns in two different variables over North American and European domains. We are thus explicitly including information on both the SLP and the impact variables. The 50 highest trivariate coupling days display anomalies consistent with those in Fig. 3, albeit somewhat weakened (Fig. 4). The large-scale SLP patterns are comparable to those conditioned on the occurrence of compound cold–wet–windy extremes (Fig. S6). A sensitivity test on broader SLP domains over both North America and Europe is shown in Fig. S7. The link between the high-coupling days and the compound extremes is again stronger over Europe, although for compound cold–wet extremes there is a high sign agreement also over North America (Table S1). We do not present here the alpha anomalies associated with extremes in an impact variable as we now consider more than one impact variable simultaneously in computing the coupling.

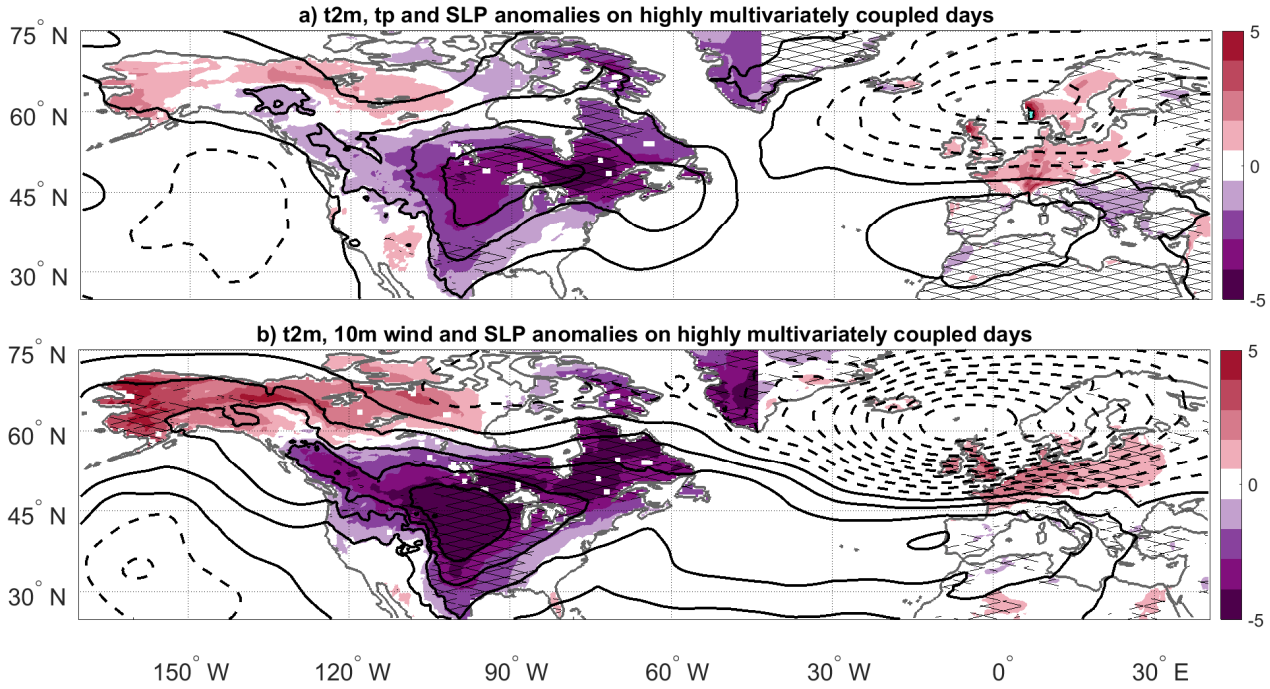

Figure 4. Multivariate coupling between SLP and impact variables in North America and Europe. As Fig. 3 but for (a) $\alpha_{SLP,t2m,tp}$ and (b) $\alpha_{SLP,t2m,10m\_wind}$, where SLP is taken jointly over 30–45 °N 260–290 °E and 45–60 °N 350–20 °E.

5 Discussion and Conclusions

We implemented a recently-developed approach from dynamical systems theory, termed *co-recurrence ratio*, to study the co-occurrence of cold spells in Eastern North America and wet or windy extremes in Western Continental Europe. It has previously been hypothesised that these events are statistically and physically linked (Messori *et al.*, 2016; De Luca *et al.*, 2020a). In our analysis, we presented the first implementation of the co-recurrence ratio in a trivariate setting. We framed the study around two questions, namely: whether the individual extreme event classes of interest emerge as having a particularly strong coupling to large-scale atmospheric patterns; and whether there is evidence for recurrent large-scale circulation patterns linking the co-occurrence of these extremes in North America and Europe.

The co-recurrence ratio indicates that both cold spells in Eastern North America and wet or windy extremes in Western Continental Europe show an unusually strong coupling to recurrent large-scale atmospheric patterns. Consistent with past literature, the key large-scale features are an anomalous ridge over central North America and an anomalous NAO-like dipole between the North Sea and the Mediterranean. Concerning the second question, our analysis suggests a

nuanced picture. Days when the SLP patterns over North America and Europe are strongly coupled display spatially coherent cold North American anomalies and wet or windy European anomalies, as well as a large-scale circulation resembling that individually associated with cold extremes in North America and wet or windy extremes in Europe. Nonetheless, the link between days when the SLP patterns over North America and Europe are strongly coupled and extremes in the impact variables we consider is modest. Explicitly including the impact variables in the coupling analysis, by computing a trivariate co-recurrence ratio (between SLP and two of the impact variables at a time), does not significantly increase the link. Nonetheless, the large-scale atmospheric pattern on days with a high trivariate co-recurrence ratio is consistent with the zonal, intense jet that Messori *et al.* (2016) hypothesised was key to connecting surface anomalies across the North Atlantic (Fig. S8). We thus conclude that compound cold–wet–windy anomalies are closely associated with a recurrent large-scale atmospheric pattern grounded in a strong coupling between SLP fields over North America and Europe. The same holds to some extent for compound cold–wet–windy extremes, albeit with a weaker signal. The fact that the individual extreme event classes display a stronger coupling to the circulation than the compound extremes suggests that the latter may be associated with a more varied range of large-scale physical drivers. A complementary hypothesis is that synoptic-scale drivers which are only indirectly reflected in the large-scale picture – such as extratropical cyclones in the North Atlantic – may modulate the extreme events' co-occurrence.

Methodologically, our analysis provides a strong complement to more complex multivariate spatial extreme value statistical models. It is time-resolved, and as such enables conditioning on the occurrence of the extremes. Computing the co-recurrence ratio only requires defining one parameter, namely the percentile defining what a *recurrence* is (see Text S1). In the future, the same approach may be extended to study lagged co-recurrence, which would allow to make causality statements. As all approaches, our analysis also displays some caveats. One is the dependence of the quantitative results on the choice of geographical domain. The co-recurrence ratio uses information from the full geographical domain considered, and larger domains will contain information about atmospheric patterns which have little connection with the extremes of interest, and which dilutes the sharpness of the information provided by the co-recurrence ratio. Additionally, the theoretical grounding of the calculation of the co-recurrence ratio may pose

some challenges to interpreting the results for those not familiar with the founding concepts of dynamical systems theory.

To conclude, our findings contribute to fill existing knowledge gaps on compound cold–wet–windy extremes in North America and Europe, by considering explicitly extremes in both continents and the associated atmospheric circulation patterns. Cold spells in Eastern North America and wet or windy extremes in Western Continental Europe are connected, yet are governed by a single set of coherent atmospheric circulation patterns. This motivates further analyses focussing specifically on the statistics and drivers of the compound extremes. We further conclude that the co-recurrence ratio can provide useful insights for the study of compound climate extremes, and that several promising additional developments of the methodology exist.

Acknowledgments

The authors have no conflicts of interest nor financial conflicts related to this work.

Open Research

The ERA5 data used in this study is freely available from the Copernicus Climate Change service at:

https://cds.climate.copernicus.eu/cdsapp#!/search?type=dataset&text=ERA5

References

Brunner, M.I., Furrer, R. *and* Favre, A.-C. *(*2019*)* Modeling the spatial dependence of floods using the Fisher copula. *Hydrology and Earth System Sciences, 23,* 107–124. https://doi.org/10.5194/hess-23-107-2019

Cellitti, M. P., Walsh, J. E., Rauber, R. M., & Portis, D. H. (2006). Extreme cold air outbreaks over the United States, the polar vortex, and the large-scale circulation. *Journal of Geophysical Research: Atmospheres*, *111*(D2).

De Luca, P., Messori, G., Pons, F. M., & Faranda, D. (2020a). Dynamical systems theory sheds new light on compound climate extremes in Europe and Eastern North America. *Quarterly Journal of the Royal Meteorological Society*, *146*(729), 1636-1650.

De Luca, P., Messori, G., Faranda, D., Ward, P. J., Comou, D. (2020b) Compound warm-dry and cold-wet events over the Mediterranean. *Earth System Dynamics*, doi: 10.5194/esd-11-793-2020

Donat, M. G., Leckebusch, G. C., Pinto, J. G., & Ulbrich, U. (2010). Examination of wind storms over Central Europe with respect to circulation weather types and NAO phases. *International Journal of Climatology*, *30*(9), 1289-1300.

Faranda, D., Messori, G., and Vannitsem, S. (2019) Attractor dimension of time-averaged climate observables: insights from a low-order ocean-atmosphere model, *Tellus A, 71*, 1–11.

Faranda, D., Messori, G., & Yiou, P. (2020a). Diagnosing concurrent drivers of weather extremes: application to warm and cold days in North America. *Climate Dynamics*, *54*(3), 2187-2201.

Faranda, D., Vrac, M., Yiou, P., Jézéquel, A., & Thao, S. (2020b). Changes in future synoptic circulation patterns: Consequences for extreme event attribution. *Geophysical Research Letters*, 47, e2020GL088002. https://doi.org/10.1029/2020GL088002

Genton, M. G., Padoan, S. A., & Sang, H. (2015). Multivariate max-stable spatial processes. *Biometrika*, *102*(1), 215-230.

Gómara, I., Rodríguez-Fonseca, B., Zurita-Gotor, P., & Pinto, J. G. (2014). On the relation between explosive cyclones affecting Europe and the North Atlantic Oscillation. *Geophysical Research Letters*, *41*(6), 2182-2190.

Grotjahn, R.*, et al. (*2015*),* North American extreme temperature events and related large scale meteorological patterns: A review of statistical methods, dynamics, modeling, and trends*, Clim. Dyn.,* 1–34.

Hanley, J., & Caballero, R. (2012). The role of large-scale atmospheric flow and Rossby wave breaking in the evolution of extreme windstorms over Europe. *Geophysical Research Letters*, *39*(21).

Harnik, N., Messori, G., Caballero, R., & Feldstein, S. B. (2016). The circumglobal North American wave pattern and its relation to cold events in eastern North America. *Geophysical Research Letters*, *43*(20), 11-015.

Haylock, M. R., & Goodess, C. M. (2004). Interannual variability of European extreme winter rainfall and links with mean large-scale circulation. *International Journal of Climatology, 24*(6), 759-776.

Hersbach, H., Bell, B., Berrisford, P., Hirahara, S., Horányi, A., Muñoz-Sabater, J., ... & Thépaut, J. N. (2020). The ERA5 global reanalysis. *Quarterly Journal of the Royal Meteorological Society*, *146*(730), 1999-2049.

Hillier, J. K., & Dixon, R. S. (2020). Seasonal impact-based mapping of compound hazards. *Environmental Research Letters*, *15*(11), 114013.

Lau, W. K., & Kim, K. M. (2012). The 2010 Pakistan flood and Russian heat wave: Teleconnection of hydrometeorological extremes. *Journal of Hydrometeorology*, *13*(1), 392-403.

Laurila, T. K., Gregow, H., Cornér, J., & Sinclair, V. A. (2021). Characteristics of extratropical cyclones and precursors to windstorms in northern Europe. *Weather and Climate Dynamics, 2*(4), 1111-1130.

Lee, M. Y., C. C. Hong, *and* H. H. Hsu *(*2015*),* Compounding effects of warm sea surface temperature and reduced sea ice on the extreme circulation over the extratropical North Pacific and North America during the 2013–2014 boreal winter*, Geophys. Res. Lett., 42,* 1612–1618*,*

Liu, Y. R., Li, Y. P., Yang, X., Huang, G. H., & Li, Y. F. (2021). Development of an integrated multivariate trend-frequency analysis method: Spatial-temporal characteristics of climate extremes under global warming for Central Asia. *Environmental Research*, *195*, 110859.

Loikith, P. C., and A. J. Broccoli (2014), The influence of recurrent modes of climate variability on the occurrence of winter and summer extreme temperatures over North America, *Journal of Climate, 27*(4), 1600–1618.

Lucarini, V., Faranda, D., de Freitas, J. M. M., Holland, M., Kuna, T., Nicol, M., ... & Vaienti, S. (2016). *Extremes and recurrence in dynamical systems*. John Wiley & Sons, London.

Matthias, V., & Kretschmer, M. (2020). The influence of stratospheric wave reflection on North American cold spells. *Monthly Weather Review*, *148*(4), 1675-1690.

Messori, G., & Caballero, R. (2015). On double Rossby wave breaking in the North Atlantic. *Journal of Geophysical Research: Atmospheres*, *120*(21), 11-129.

Messori, G., Caballero, R., & Gaetani, M. (2016). On cold spells in North America and storminess in western Europe. *Geophysical Research Letters*, *43*(12), 6620-6628.

455 Messori, G., Davini, P., Alvarez-Castro, M. C., Pausata, F. S., Yiou, P., & Caballero, R. (2019).
456 On the low-frequency variability of wintertime Euro-Atlantic planetary wave-breaking. *Climate*
457 *Dynamics*, *52*(3), 2431-2450.
458
459 Messori, G. and Faranda, D. (2021). Technical note: Characterising and comparing different
460 palaeoclimates with dynamical systems theory. *Climate of the Past, 17*, 545–563,
461 https://doi.org/10.5194/cp-17-545-2021.
462
463 Messori, G., Kretschmer, M., Lee, S. H., and Matthias, V. (2022). Stratospheric Wave Reflection
464 Events Modulate North American Weather Regimes and Cold Spells, *Weather and Climate*
465 *Dynamics Discussion*, https://doi.org/10.5194/wcd-2022-18.
466
467 Naveau, P., Nogaj, M., Ammann, C., Yiou, P., Cooley, D., & Jomelli, V. (2005). Statistical
468 methods for the analysis of climate extremes. *Comptes Rendus Geoscience*, *337*(10-11), 1013-
469 1022.
470
471 Oesting, M. *and* Stein, A. *(*2018*)* Spatial modeling of drought events using max-stable processes*.*
472 *Stochastic Environmental Research and Risk Assessment, 32,* 63–81.
473
474 Owen, L. E., Catto, J. L., Stephenson, D. B., & Dunstone, N. J. (2021). Compound precipitation
475 and wind extremes over Europe and their relationship to extratropical cyclones. *Weather and*
476 *Climate Extremes*, 100342.
477
478 Palmer, T. *(*2014*),* Record-breaking winters and global climate change*, Science, 344(*6186*),* 803–
479 804*.*
480
481 Smith, E. T., & Sheridan, S. C. (2018). The characteristics of extreme cold events and cold air
482 outbreaks in the eastern United States. *International Journal of Climatology, 38*, e807-e820.
483
484 Tavakol, A., Rahmani, V., & Harrington Jr, J. (2020). Probability of compound climate extremes
485 in a changing climate: A copula-based study of hot, dry, and windy events in the central United
486 States. *Environmental Research Letters*, *15*(10), 104058.
487
488 Towler, E., Llewellyn, D., Prein, A., & Gilleland, E. (2020). Extreme-value analysis for the
489 characterization of extremes in water resources: A generalized workflow and case study on New
490 Mexico monsoon precipitation. *Weather and Climate Extremes*, *29*, 100260.
491
492 van Oldenborgh, G.J.*,* Stephenson, D.B.*,* Sterl, A.*,* Vautard, R.*,* Yiou, P.*,* Drijfhout, S.S.*,* von
493 Storch, H. *and* van den Dool, H. *(*2015*)* Drivers of the 2013/14 winter floods in the UK*. Nature*
494 *Climate Change, 5, 490–491. https://doi.org/10.1038/nclimate2612*
495
496 Vogel, J., Rivoire, P., Deidda, C., Rahimi, L., Sauter, C. A., Tschumi, E., ... & Zscheischler, J.
497 (2021). Identifying meteorological drivers of extreme impacts: an application to simulated crop
498 yields. *Earth system dynamics*, *12*(1), 151-172.
499

500 Zscheischler, J., Westra, S., Van Den Hurk, B. J., Seneviratne, S. I., Ward, P. J., Pitman, A., ... &
501 Zhang, X. (2018). Future climate risk from compound events. *Nature Climate Change*, *8*(6),
502 469-477.

Geophysical Research Letters

Supporting Information for

Diagnosing the Systematic Occurrence of Wintertime Compound Climate Extremes in North America and Europe

Gabriele Messori[1,2] Davide Faranda[3,4,5]

1. Department of Earth Sciences and Centre of Natural Hazards and Disaster Science (CNDS), Uppsala University, Uppsala, Sweden.
2. Department of Meteorology and Bolin Centre for Climate Research, Stockholm University, Stockholm, Sweden.
3. Laboratoire des Sciences du Climat et de l'Environnement, LSCE/IPSL, CEA-CNRS-UVSQ, Université Paris-Saclay, Gif-sur-Yvette, France.
4. London Mathematical Laboratory, London, UK.
5. LMD/IPSL, Ecole Normale Superieure, PSL research University, Paris, France.

Corresponding author: Gabriele Messori (gabriele.messori@geo.uu.se)

Contents of this file

Introduction

In this Supporting Information, we provide text describing in detail the computation of the co-recurrence ratio (Text S1) and text describing the algorithm to define compound extreme occurrences (Text S3). All supplementary figures and tables which complement the analysis in the main text are described in Text S2.

Text S1.

The computation of α is grounded in the concept of recurrences, widely used in dynamical systems theory. Given a long trajectory $\boldsymbol{x}(t)$ describing the evolution of a stationary chaotic dynamical system (returning to our previous example, this could be a succession of latitude-longitude t2m or SLP maps), one can define logarithmic returns relative to a specific state of interest ζ_x (a t2m or SLP map on a specific day) as:

$$g(\boldsymbol{x}(t),\zeta_x)=-\log[\mathrm{dist}(\boldsymbol{x}(t),\zeta_x)]$$

Here *dist* is a distance function between two vectors, that tends to zero for increasing resemblance. We use the Euclidean distance; the implications of using other distance functions are discussed in Lucarini *et al.* (2016) and Faranda *et al.* (2019). Using the –log function makes the timeseries g large when *dist* is small, namely when we observe a recurrence such that $\boldsymbol{x}(t)$ resembles ζ_x. We next select a threshold $s(q,\zeta_x)$, where q is a high quantile of $g(\boldsymbol{x}(t),\zeta_x)$ (here q=0.98). We define recurrences of ζ_x as timesteps t_i at which $g(\boldsymbol{x}(t_i),\zeta_x) > s(q,\zeta_x)$.

Given a second trajectory $\boldsymbol{y}(t)$ and a state of interest ζ_y one can similarly define a series $g(\boldsymbol{y}(t),\zeta_y)$, a high threshold $s(q,\zeta_y)$ and a joint state of interest $\zeta=(\zeta_x,\zeta_y)$. For simplicity, we hereafter drop the ζ_x and ζ_y from our notation and append the variables as subscripts. The co-recurrence ratio is then given by:

$$\alpha_{x,y}(\zeta) = \frac{\nu[g(\boldsymbol{x}(t)) > s_x(q) \cap g(\boldsymbol{y}(t)) > s_y(q)]}{\nu[g(\boldsymbol{x}(t)) > s_x(q)]}$$

Here $\nu[-]$ denotes the number of events satisfying condition $[-]$, and $0 \leq \alpha \leq 1$. By defining the high thresholds as quantiles of the series g, we implicitly impose that $\nu[g(\boldsymbol{x}(t))>s_x(q)] \equiv \nu[g(\boldsymbol{y}(t))>s_y(q)]$. Thus, α is independent of the ordering of the variables, and may not be interpreted in terms of causality. For atmospheric variables, α typically takes values of order of 10^{-2} to 10^{-1} (Faranda *et al.*, 2020a; De Luca *et al.*, 2020a, b; Messori and Faranda, 2021). The choice of a high $s(q,\zeta_y)$ to define recurrence implies that these are inherently rare, as are joint recurrences. Thus, even relatively low fractions of joint recurrences are very unlikely to be obtained by chance. As an example, the $\alpha_{t2m,SLP}$ discussed in Sect. 4.1 ranges over $0 \leq \alpha \leq 0.37$, while the $\alpha_{SLP1,SLP2}$ discussed in Sect. 4.2 ranges over $0 \leq \alpha \leq 0.13$.

The framework for joint recurrences may be extended to three variables. Given a third trajectory $\boldsymbol{z}(t)$ and $\zeta=(\zeta_x,\zeta_y,\zeta_z)$, one may define:

$$\alpha_{x,y,z}(\zeta) = \frac{\nu[(g(\boldsymbol{x}(t)) > s_x(q) \cap g(\boldsymbol{y}(t)) > s_y(q)) \cap g(\boldsymbol{z}(t)) > s_z(q)]}{\nu[g(\boldsymbol{x}(t)) > s_x(q)]}$$

Even in this case, α is independent of the ordering of the variables. One simply poses the additional constraint of a third, simultaneous co-recurrence. This suggests that a trivariate α will display lower values than its bivariate counterpart. As an example, the $\alpha_{SLP,t2m,10m\_wind}$ discussed in Sect. 4.2 ranges over $0 \leq \alpha \leq 0.07$. We underscore that a joint recurrence across three variables is an extremely stringent condition, such that the trivariate alpha attains low values almost by design. Even seemingly low values are therefore highly unlikely to be obtained by chance.

Text S2.

In the supplementary material we present: a table showing co-recurrence ratio anomalies during compound extremes; figures showing the SLP, t2m, tp and 10m wind composite anomalies for cold spells, tp, 10m wind and compound extremes in the North American and European domains we analyse here (Figs. S1, S6); a figure testing the correspondence between high-coupling days and (near-)surface extremes (Fig. S2); figures testing the sensitivity of our results to the choice of geographical domain (Figs.

S3—5, 7); and a figure showing the upper-level flow anomalies associated with the high coupling days shown in Fig. 4 (Fig. S8).

In Figs. S5 and S7, several of the key large-scale features identified in Figs. 3 and 4 are still evident, but the strong negative t2m signal over North America is partially lost. This is not surprising: we are simultaneously extending the SLP domains over both North America and Europe, which adds significant information that may not be directly relevant to extreme occurrences in the domains of interest, and pushes the limits of the co-recurrence ratio.

Fig. S8 shows a stronger signal on the jet stream of the co-recurrence ratio computed on 10m wind rather than on tp. We speculate that this may depend on the fact that windstorms are more closely associated with North Atlantic cyclones than heavy precipitation, which can also be associated with other drivers (*e.g.* lake effect in the Baltic region).

Text S3.

Compound extremes in Table S1 and Fig. S6 are identified as area-averaged t2m extremes in Eastern North America (45–60 °N 350–20 °E), which occur within 5 days of a tp or 10m wind extreme in Western Continental Europe (45–60 °N 350–20 °E). The compound extremes are ordered according to the joint rank of the two impact variables being considered. For example, the 20^{th} coldest cold spell matching the 30^{th} heaviest precipitation event will be assigned a joint rank of 50; similarly, the 10^{th} coldest cold spell matching the 32^{nd} heaviest precipitation event will be assigned a joint rank of 42 etc. The top 50 compound cold–wet and cold–windy extremes according to joint rank are then selected.

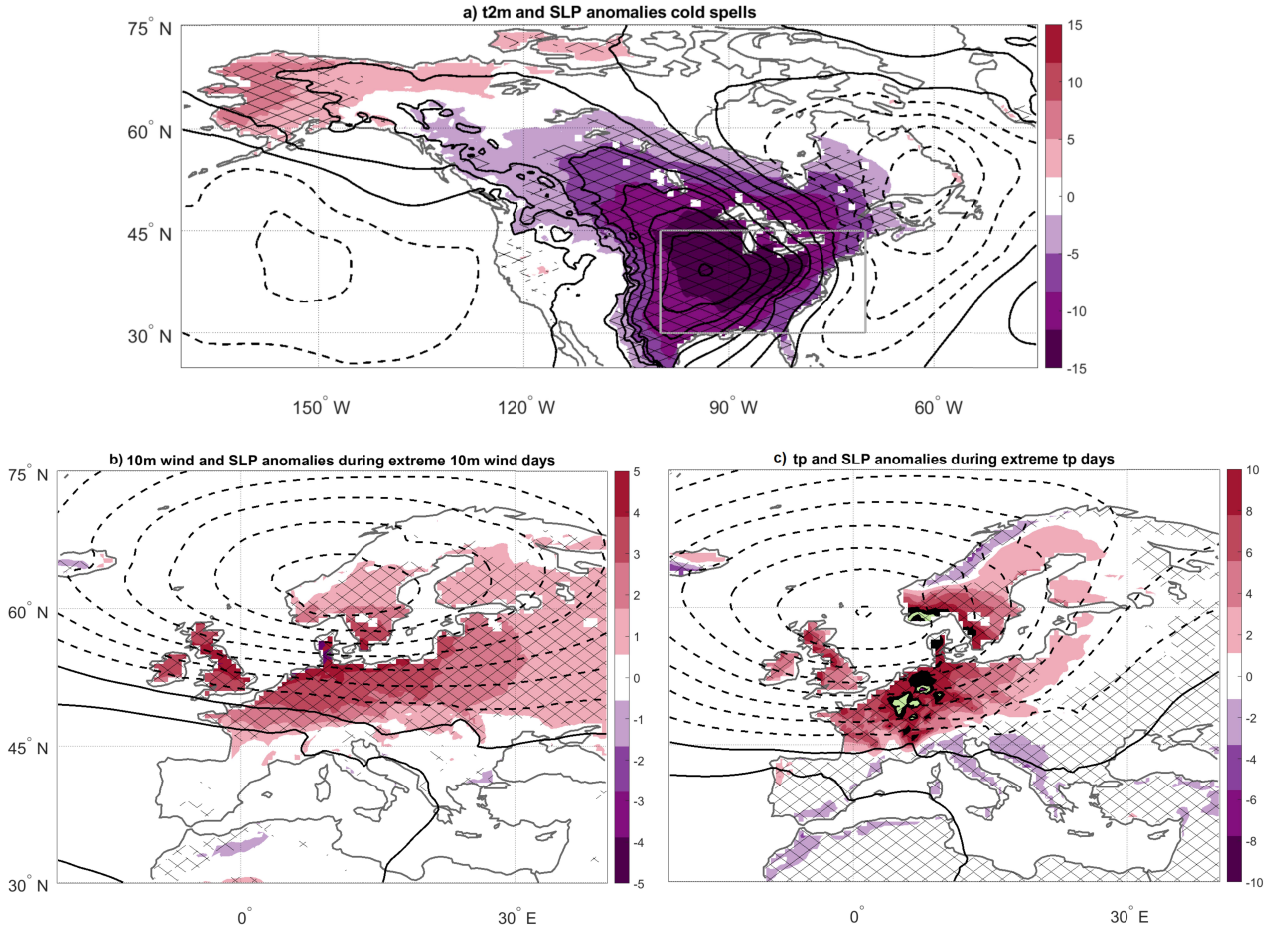

Figure S1. (a) 2-metre temperature (t2m, K, colours) and sea-level pressure (SLP, hPa, contours) anomalies for the 50 coldest cold spells over Eastern North America (grey box in Fig. 1a, 30–45 °N 260–290 °E). (b) Same as (a) but for the 50 strongest 10-metre wind (10m wind, m s^{-1}) events over Europe (grey box in Fig. 2a, 45–60 °N 350–20 °E). (c) Same as (b) but for the 50 heaviest total precipitation (tp, mm day^{-1}, colours) events.

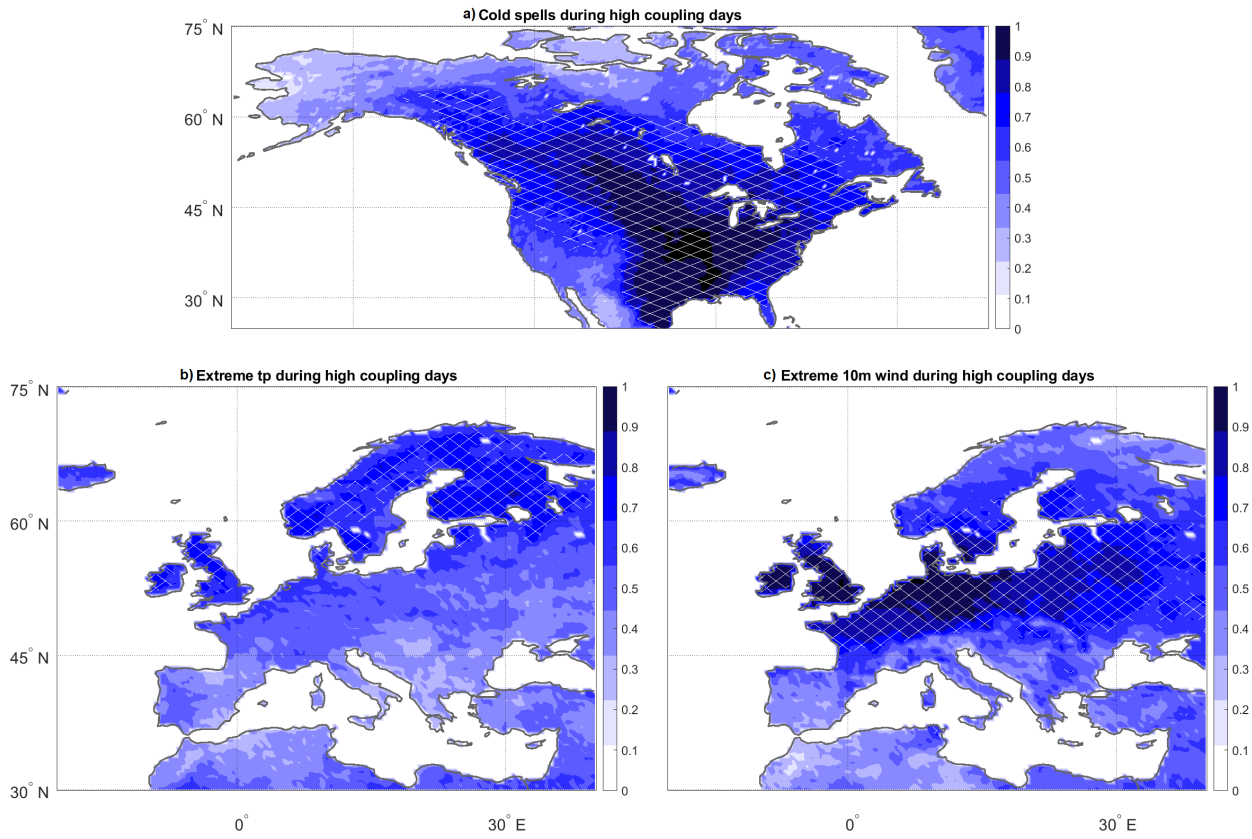

Figure S2. Correspondence between the 50 days displaying the highest coupling and (near-)surface extremes (ranked by area-averaged anomalies over 45–60 °N 350–20 °E (t2m) or 30–45 °N 260–290 °E (tp and 10m wind)). (a) Normalised occurrence of cold spells during high $\alpha_{t2m,SLP}$ computed over 30–45 °N 260–290 °E. (b) Normalised occurrence of extreme tp during high $\alpha_{tp,SLP}$ computed over 45–60 °N 350–20 °E. (c) Same as (b) but for extreme 10m wind and $\alpha_{10m\_wind,SLP}$. All extremes are defined as the top (bottom for t2m) 5 percentiles of the local distributions, imposing a minimum separation between extremes of 5 days. A high α value is considered to match an extreme if the latter falls within 5 days of the former. The number of extremes occurring during high α days is then normalised to [0, 1]. Cross-hatching marks regions where the occurrence of extremes during high α days is significantly higher than climatology at the 5% one-sided level, determined using 1000 random sampling iterations.

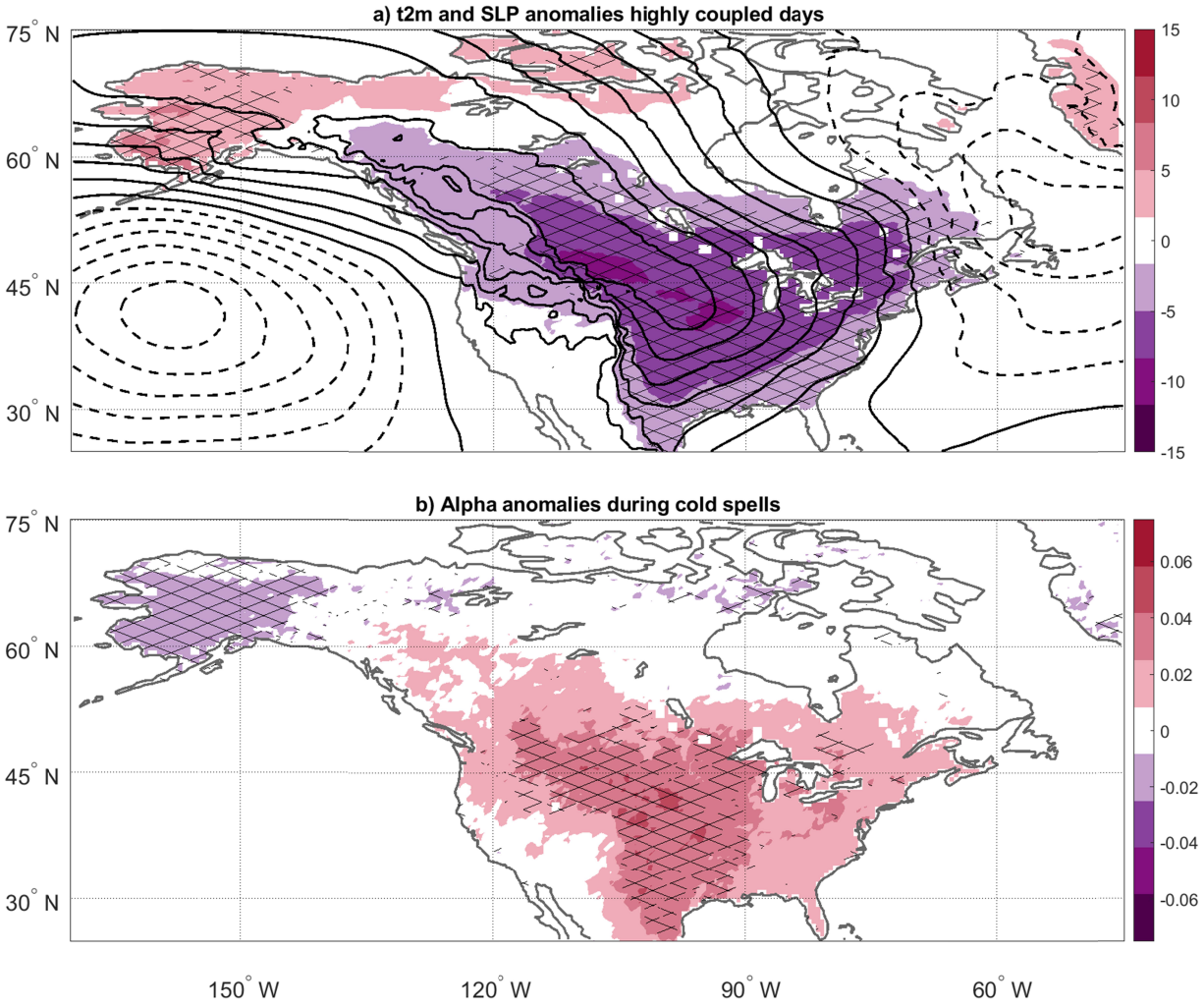

Figure S3. Same as Fig. 1 but for $\alpha_{t2m,SLP}$ computed using SLP over 25–75 °N 190–315 °E. Note that the colourscale in panel (b) is different from that in Fig. 1b.

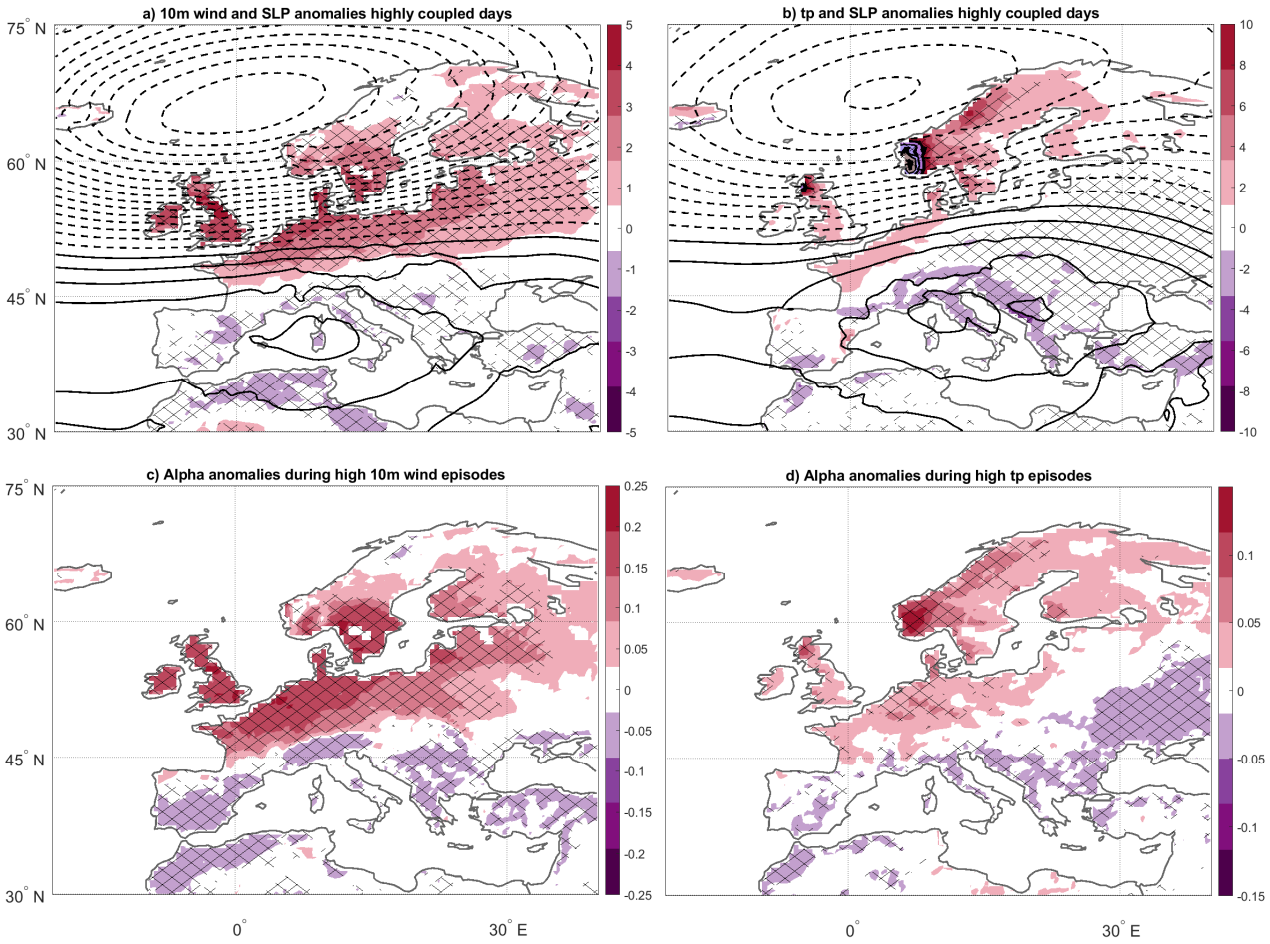

Figure S4. Same as Fig. 2 but for $\alpha_{10m\ wind,SLP}$ and $\alpha_{tp,SLP}$ computed using SLP over 30–75 °N 340–40 °E. Note that the colourscale in panel (c) is different from that in Fig. 2c.

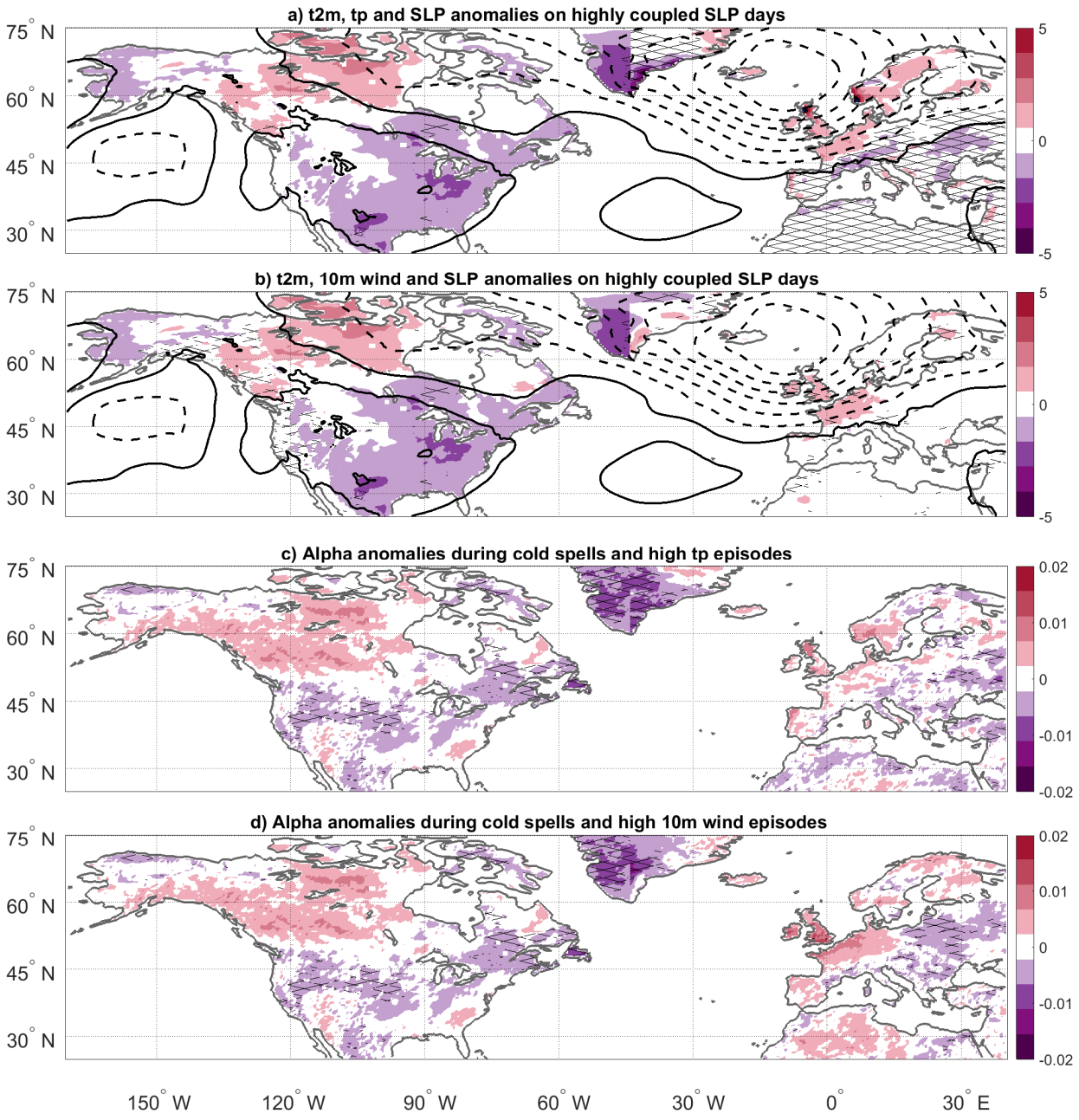

Figure S5. Same as Fig. 3 but for $\alpha_{SLP1,SLP2}$ computed using SLP over 25–75 °N 190–315 °E and 30–75 °N 340–40 °E.

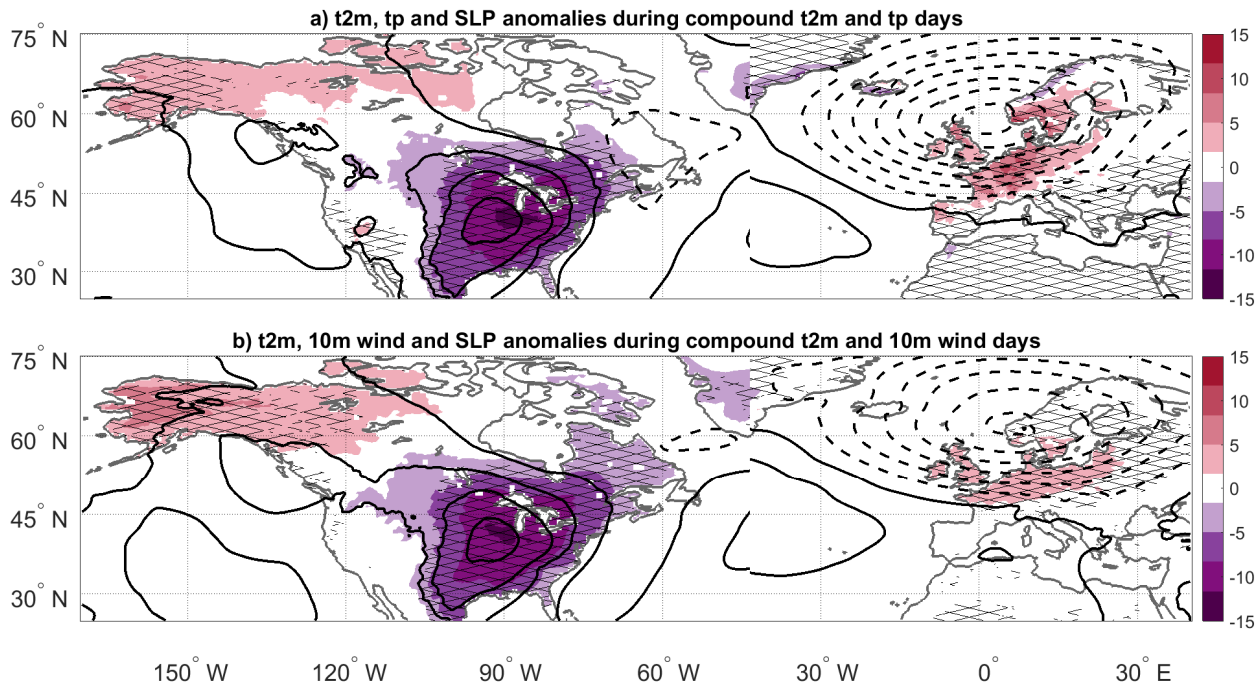

Figure S6. (a) 2-metre temperature (t2m, K) and total precipitation (tp, mm day^{-1}) anomalies in colours in the left and right-hand sides of the panel, respectively. Sea-level pressure (SLP, hPa) anomalies are shown in contours every 2 hPa, with negative contours dashed. Anomalies are composited over the 50 strongest compound cold–wet extremes over Eastern North America (grey box in Fig. 1a, 30–45 °N 260–290 °E) and Western Continental Europe (grey box in Fig. 2a, 45–60 °N 350–20 °E). (b) Same as (a) but for 10-metre wind (10m wind, m s^{-1}) and for the 50 strongest compound cold–windy extremes. Since this approach allows up to a 5-day shift between the left and right-hand sides of the panels (see Text S3), unlike in other figures the SLP contours do not match at the boundary between the t2m and tp or 10m wind domains.

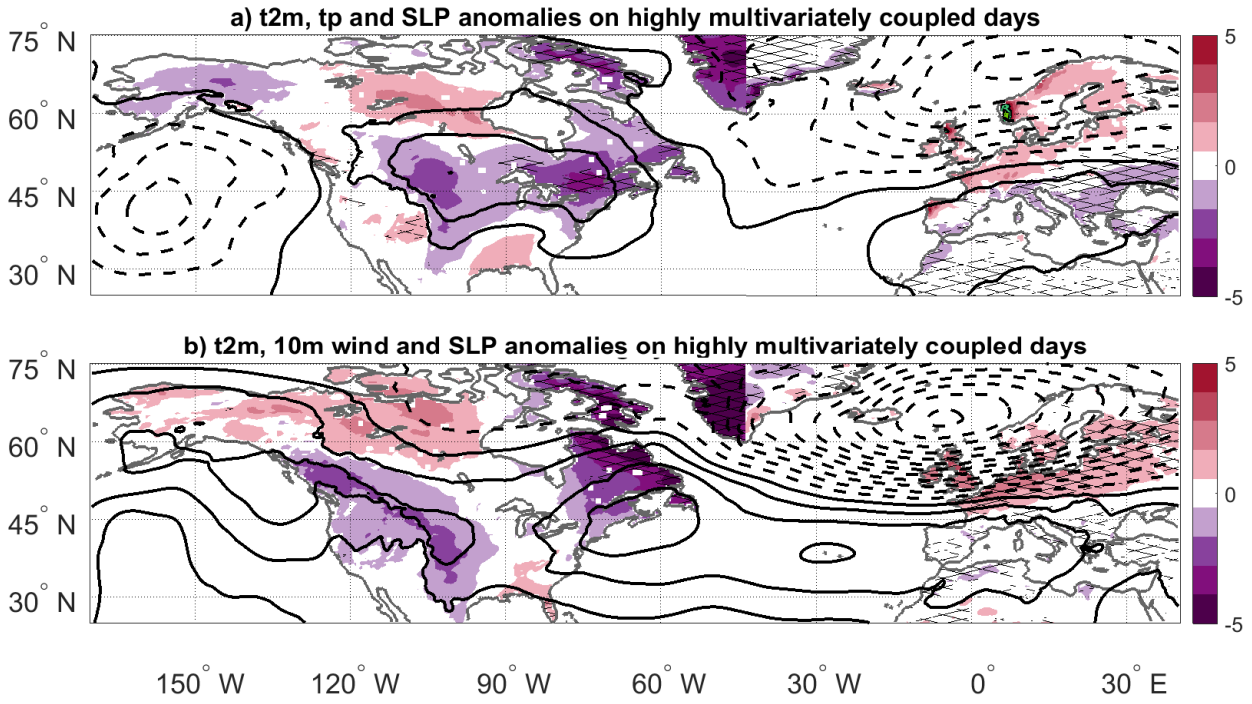

Figure S7. Same as Fig. 4 but for $\alpha_{SLP,t2m,tp,}$ and $\alpha_{SLP,t2m,10m\_wind}$ computed using SLP over 25–75 °N 190–315 °E and 30–75 °N 340–40 °E.

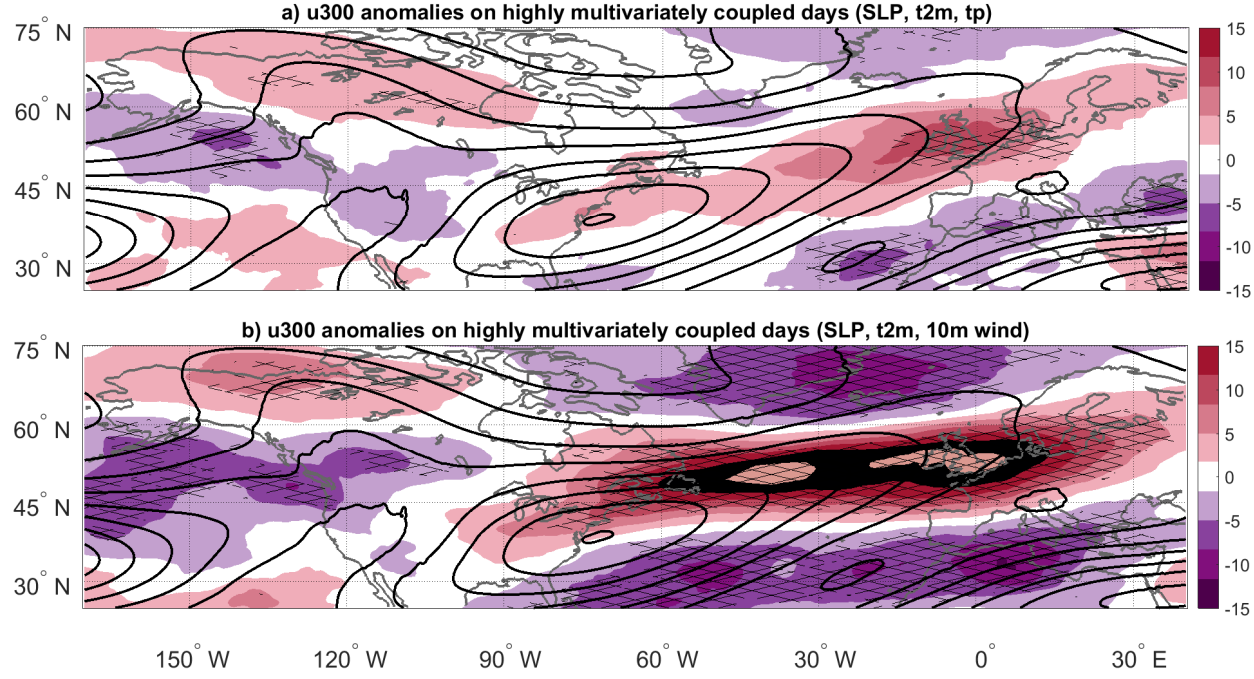

Figure S8. 300 hpa zonal wind anomalies (u300, m s^{-1}, colours) and climatological DJF zonal wind (contours, every 2 m s^{-1}) during the 50 highest (a) $\alpha_{SLP,tp,SLP}$ and (b) $\alpha_{SLP,10m\_wind,SLP}$ days. Both α are computed over the same domains as in Fig. 4. Cross-hatching marks regions where at least two thirds of the u300 anomalies share the same sign.

Table S1. α anomalies during compound extremes, defined as in Text S3. All values are rounded to two decimal places. Since the dates of the North American t2m and European tp or 10m wind events within each compound extreme can differ by up to 5 days, separate α anomalies for North America and Europe are provided for each α variable. Numbers in bold indicate that more than 2/3 of the α anomalies for the individual compound extremes share the same sign.

α variable	**Type of Compound Extreme**			
	Cold—Wet		**Cold—Windy**	
	α anomaly North America	**α anomaly Europe**	**α anomaly North America**	**α anomaly Europe**
$\alpha_{SLP1,SLP2}$ as in Fig. 3	0.01	**0.02**	0.01	**0.02**
$\alpha_{SLP,t2m,tp}$ as in Fig. 4	**0.01**	**0.01**	**—**	**—**
$\alpha_{SLP,t2m,10m\_wind}$ as in Fig. 4	**—**	**—**	0.01	**0.01**